Author's personal copy

International Journal of Heat and Mass Transfer 53 (2010) 2424–2433

Contents lists available at ScienceDirect

International Journal of Heat and Mass Transfer

journal homepage: www.elsevier.com/locate/ijhmt

A macroscopic two-energy equation model for turbulent flow and heat transfer in highly porous media

Marcelo B. Saito, Marcelo J.S. de Lemos *

Departamento de Energia – IEME, Instituto Tecnológico de Aeronáutica – ITA, 12228-900 São José dos Campos – SP, Brazil

ARTICLE INFO

Article history:
Received 22 May 2009
Received in revised form 15 December 2009
Accepted 15 December 2009
Available online 15 February 2010

Keywords:
Turbulence modeling
Porous media
Two-energy equation

ABSTRACT

In this paper, a model for turbulent flow and heat transfer in a highly porous medium is proposed and applied to a porous channel bounded by parallel plates. Macroscopic continuity, momentum and energy equations are presented. Local non-thermal equilibrium is considered by means of independent equations for the solid matrix and the working fluid. The numerical methodology used is based on the control-volume approach. The effects of thermal dispersion, Reynolds number, dimensionless particle diameter, thermal conductivity ratio and Darcy number, on the Nusselt number, are presented. For laminar and turbulent flows the thermal dispersion mechanism leads to larger local temperature differences. Increase in *Re* number causes values for *Nu*, of both phases, to increase. Porosity increase causes the solid phase Nusselt number to decrease whereas the fluid Nusselt number in augmented. In general, an increase in the particle diameter increases Nusselt number. Also, the thermal conductivity ratio causes the most pronounced effect on Nusselt numbers.

© 2010 Elsevier Ltd. All rights reserved.

1. Introduction

The ability to simulate turbulent flow and heat transfer in permeable media has many industrial and environment applications, such as analyses of chemical reactors, groundwater flow, fluidized bed combustion, grain storage, dryers, energy storage units and gas flow in reservoirs, to mention a few.

For highly porous media, or say, when the void space within the pores corresponds to about 80–95% of the total volume (fluid and solid), additional modeling difficulties arise due to the fact that turbulence might exist in the fluid phase. The literature recognizes that such condition appears when the Reynolds number based on the statistical pore size, Re_D, is higher than around 300.

Further, when analyzing heat transfer in porous media, there are basically two approached to follow. One can assume thermal equilibrium between the solid matrix and the working fluid (local thermal equilibrium model – LTE), or else, one can analyze each phase with an independent energy balance equation (local non-thermal equilibrium model – LNTE).

The hypothesis of local thermal equilibrium (LTE) demands several constraints which have been considered by a number of authors [1–6]. For instance, the LTE hypothesis is no longer valid when the particles or pores are not small enough, when the thermal properties differ widely, or when convective transport is not important. Also, most recent papers on the effects of local thermal non-equilibrium deal with unsteady situations [7,8], which are here not considered. Further, when there is a significant heat generation in any of the phases, the system will rapidly depart from the local thermal equilibrium condition [9]. For such extreme conditions, the one-energy equation model (LTE) is inadequate to correctly describe both the transients associated with the quench front penetrating the hot dry porous layer, as well as regions where dry out occurs.

As mentioned, when the assumption of local thermal equilibrium fails, one possible solution is to develop separate transport equations for each phase [10–12] and this leads to macroscopic models, which are referred to in the literature as LNTE closures. For heat transport through a porous medium, a LNTE model involves the derivation of energy equation for both the solid and the fluid, which, in turn, requires additional information on the interfacial heat transfer coefficient between the fluid phase and the solid phase [13,14]. For that, the use of LNTE models is, on the whole, more involving [15].

Further, if the flow is turbulent, additional difficulties arise due to the fact that the flow properties fluctuate with time and vary with location within the medium [16]. To handle such cases, proposals for treating turbulent flow in porous media have been presented in the literature [17,18] as well as a review on turbulence modeling in porous structures [19]. Significant contributions have also been made by other groups [20,21].

In this paper, we extend a macroscopic model that has been developed and published in a series of papers [22–24], which were based on the two-equation turbulence model of [25] but considered

* Corresponding author.
E-mail address: delemos@ita.br (M.J.S. de Lemos).

0017-9310/$ - see front matter © 2010 Elsevier Ltd. All rights reserved.
doi:10.1016/j.ijheatmasstransfer.2010.01.041

Author's personal copy

Nomenclature

Latin characters

A_i	interface total area between the fluid and solid
c_F	Forchheimer coefficient
c_p	fluid specific heat
D	particle or rod diameter
Da	Darcy number, $Da = K/H^2$
h_i	interfacial heat transfer coefficient
$\boldsymbol{H}$	channel height
$\mathbf{I}$	unit tensor
K	permeability
k	turbulence kinetic energy per unit mass
k_f	fluid thermal conductivity
k_s	solid thermal conductivity
$\mathbf{K}_{disp}$	dispersion tensor
$\mathbf{K}_{f,s}$	thermal conductivity tensor for fluid phase
$\mathbf{K}_{s,f}$	thermal conductivity tensor for solid phase
$\mathbf{K}_t$	turbulent diffusion tensor
$\mathbf{K}_{disp,t}$	turbulent dispersion tensor
$\boldsymbol{L}$	channel length
p	pressure
Pr	$Pr = \nu/\alpha$, Prandtl number
Re_D	Reynolds number based on D and superficial velocity $\bar{\mathbf{u}}_D$
T	temperature
$\overline{T}$	time averaged temperature
$\mathbf{u}$	local instantaneous velocity
$\bar{\mathbf{u}}_D$	time-mean Darcy or superficial velocity (time-volume average of $\mathbf{u}$)
Y	$Y = y/H$, dimensionless transversal coordinate
X	$X = x/H$, dimensionless longitudinal coordinate

Greek characters

α	fluid thermal diffusivity
ΔV	representative elementary volume
ΔV_f	fluid volume inside ΔV
μ	fluid dynamic viscosity
μ_t	eddy viscosity
μ_{t_ϕ}	macroscopic eddy viscosity
ν	fluid kinematic viscosity
ρ	fluid density
ϕ	$\phi = \Delta V_f/\Delta V$, porosity
θ	$\theta_{(s,f)} = \frac{T_w - T}{T_w - T_{inlet_{(s,f)}}}$, dimensionless local temperature
Θ	$\Theta_{(s,f)} = \frac{T_{m_{(s,f)}} - T_{inlet_f}}{T_{inlet_s} - T_{inlet_f}}$, Dimensionless bulk temperature

Special characters

φ	general variable
$\langle\varphi\rangle i$	intrinsic average
$\langle\varphi\rangle v$	volume average
${}^i\varphi$	spatial deviation

Subscripts

B	bulk
w	wall

both time fluctuations and space deviation of all variables involved. That technique has been extended to non-buoyant heat transfer [26], buoyant flows [27–31], mass transfer [32], double-diffusive transport [33] and to hybrid (porous/clear) media [34,35]. Recently, the specific problem of treating interfaces between a finite porous medium and a surrounding free-flow region, considering a diffusion-jump condition for both laminar [36] and turbulence fields [37–39], have also been investigated under the concept first proposed by [22–24]. These applications are here reviewed in order to give a broader view on the work already published in this field.

Following the concept proposed in [22], de Lemos and Rocamora [40] developed a macroscopic energy equation for porous medium, considering local thermal equilibrium (LTE) between the fluid and solid matrix. Later, Saito and de Lemos [41] proposed a correlation for the interfacial heat transfer coefficient for turbulent flow in an infinite staggered array of square rods. In a recent paper [42], laminar flow through a porous reactor has been simulated, using correlations for laminar interfacial heat transfer [13,14]. However, in none of the above mentioned works, models for macroscopic turbulent flow, including the LNTE closure, have been combined to analyze heat transfer in a porous bed.

The objective of the present contribution is to present computations for a full two-energy equation model, which combines the interfacial heat transfer correlation given by [41] and the turbulent flow model of [22–24]. As such, the range of application of LNTE models for porous media is extended from pure laminar [15,42] to fully turbulent [41] flow regime.

2. Mathematical modeling

2.1. Local instantaneous transport equations

The governing equations for the flow and energy for an incompressible fluid are given by:

$$\text{Continuity:}\quad \nabla\cdot\mathbf{u} = 0 \tag{1}$$

$$\text{Momentum:}\quad \rho\left[\frac{\partial\mathbf{u}}{\partial t} + \nabla\cdot(\mathbf{u}\,\mathbf{u})\right] = -\nabla p + \mu\nabla^2\mathbf{u} \tag{2}$$

$$\text{Energy-Fluid Phase:}\quad (\rho c_p)_f\left\{\frac{\partial T_f}{\partial t} + \nabla\cdot(\mathbf{u}T_f)\right\} = \nabla\cdot(k_f\nabla T_f) + S_f \tag{3}$$

$$\text{Energy-Solid Phase (Porous Matrix):}\quad (\rho c_p)_s\frac{\partial T_s}{\partial t} = \nabla\cdot(k_s\nabla T_s) + S_s \tag{4}$$

where the subscripts f and s refer to fluid and solid phases, respectively. Here, T is the temperature, k_f and k_s are the fluid and solid thermal conductivities, respectively, c_p is the specific heat and S is the heat generation term. If there is no heat generation either in the solid or in the fluid, one has $S_f = S_s = 0$.

2.2. Double-decomposition of variables

Macroscopic transport equations for turbulent flow in a porous medium are obtained through the simultaneous application of time and volume average operators over a generic fluid property φ. Such concepts are defined as [22–24].

$$\bar{\varphi} = \frac{1}{\Delta t}\int_t^{t+\Delta t}\varphi\,dt, \quad \text{with}\ \ \varphi = \bar{\varphi} + \varphi' \tag{5}$$

$$\langle\varphi\rangle^i = \frac{1}{\Delta V_f}\int_{\Delta V_f}\varphi\,dV; \qquad \langle\varphi\rangle^v = \phi\langle\varphi\rangle^i;$$

$$\phi = \frac{\Delta V_f}{\Delta V}, \quad \text{with}\ \ \varphi = \langle\varphi\rangle^i + {}^i\varphi \tag{6}$$

Author's personal copy

where ΔV_f is the volume of the fluid contained in a representative elementary volume (REV) ΔV, intrinsic average and volume average are represented, respectively, by $\langle\rangle^i$ and $\langle\rangle^v$. The double decomposition idea, introduced and fully described in [22–24], combines Eqs. (5) and (6) and can be summarized as:

$$\overline{\langle\varphi\rangle^i} = \langle\bar{\varphi}\rangle^i; \qquad {}^i\bar{\varphi} = \overline{{}^i\varphi}; \qquad \langle\varphi'\rangle^i = \langle\varphi\rangle^{i'} \tag{7}$$

and,

$$\left.\begin{aligned} \varphi' &= \langle\varphi'\rangle^i + {}^i\varphi' \\ {}^i\varphi &= \overline{{}^i\varphi} + {}^i\varphi' \end{aligned}\right\} \quad \text{where } {}^i\varphi' = \varphi' - \langle\varphi'\rangle^i = {}^i\varphi - \overline{{}^i\varphi} \tag{8}$$

Therefore, the quantity φ can be expressed by either,

$$\varphi = \overline{\langle\varphi\rangle^i} + \langle\varphi\rangle^{i'} + \overline{{}^i\varphi} + {}^i\varphi' \tag{9}$$

or

$$\varphi = \langle\bar{\varphi}\rangle^i + {}^i\bar{\varphi} + \langle\varphi'\rangle^i + {}^i\varphi' \tag{10}$$

The term ${}^i\varphi'$ can be viewed as either the temporal fluctuation of the spatial deviation or the spatial deviation of the temporal fluctuation of the quantity φ.

2.3. Macroscopic flow equations

When the average operators (5) and (6) are simultaneously applied over Eqs. (1) and (2), macroscopic equations for turbulent flow are obtained. Volume integration is performed over a REV [16,42], resulting in,

$$\text{Continuity}: \quad \nabla\cdot\bar{\mathbf{u}}_D = 0 \tag{11}$$

where $\bar{\mathbf{u}}_D = \phi\langle\bar{\mathbf{u}}\rangle^i$ and $\langle\bar{\mathbf{u}}\rangle^i$ identifies the intrinsic (liquid) average of the time-averaged velocity vector $\bar{\mathbf{u}}$.

Momentum:

$$\rho\left[\frac{\partial\bar{\mathbf{u}}_D}{\partial t} + \nabla\cdot\left(\frac{\bar{\mathbf{u}}_D\,\bar{\mathbf{u}}_D}{\phi}\right)\right] = -\nabla\left(\phi\langle\bar{p}\rangle^i\right) + \mu\nabla^2\bar{\mathbf{u}}_D - \nabla\cdot\left(\rho\phi\langle\overline{\mathbf{u}'\mathbf{u}'}\rangle^i\right) - \left[\frac{\mu\phi}{K}\bar{\mathbf{u}}_D + \frac{c_F\phi\rho|\bar{\mathbf{u}}_D|\bar{\mathbf{u}}_D}{\sqrt{K}}\right] \tag{12}$$

where the last two terms in Eq. (12) represent the Darcy and Forchheimer or form drags. The symbol K is the porous medium permeability, c_F is the form drag or Forchheimer coefficient, $\langle\bar{p}\rangle^i$ is the intrinsic average pressure of the fluid and φ is the porosity of the porous medium.

The macroscopic Reynolds stress, $-\rho\phi\langle\overline{\mathbf{u}'\mathbf{u}'}\rangle^i$, appearing in Eq. (12) is given as,

$$-\rho\phi\langle\overline{\mathbf{u}'\mathbf{u}'}\rangle^i = \mu_{t_\phi}2\langle\bar{\mathbf{D}}\rangle^{\mathbf{v}} - \frac{2}{3}\phi\rho\langle k\rangle^i\mathbf{I} \tag{13}$$

where

$$\langle\bar{\mathbf{D}}\rangle^v = \frac{1}{2}\left[\nabla\left(\phi\langle\bar{\mathbf{u}}\rangle^i\right) + \left[\nabla(\phi\langle\bar{\mathbf{u}}\rangle^i)\right]^T\right] \tag{14}$$

is the macroscopic deformation tensor, $\langle k\rangle^i = \langle\overline{\mathbf{u}'\cdot\mathbf{u}'}\rangle^i/2$ is the intrinsic turbulent kinetic energy, and μ_{t_ϕ}, is the turbulent viscosity, which is modeled in [23] similarly to the case of clear flow, in the form,

$$\mu_{t_\phi} = \rho c_\mu\frac{\langle k\rangle^{i^2}}{\langle\varepsilon\rangle^i} \tag{15}$$

The intrinsic turbulent kinetic energy per unit mass and its dissipation rate are governed by the following equations:

$$\rho\left[\frac{\partial}{\partial t}(\phi\langle k\rangle^i) + \nabla\cdot(\bar{\mathbf{u}}_D\langle k\rangle^i)\right] = \nabla\cdot\left[\left(\mu + \frac{\mu_{t_\phi}}{\sigma_k}\right)\nabla(\phi\langle k\rangle^i)\right] - \rho\langle\overline{\mathbf{u}'\mathbf{u}'}\rangle^i\nabla\bar{\mathbf{u}}_D + c_k\rho\frac{\phi\langle k\rangle^i|\bar{\mathbf{u}}_D|}{\sqrt{K}} - \rho\phi\langle\varepsilon\rangle^i \tag{16}$$

$$\rho\left[\frac{\partial}{\partial t}\left(\phi\langle\varepsilon\rangle^i\right) + \nabla\cdot(\bar{\mathbf{u}}_D\langle\varepsilon\rangle^i)\right] = \nabla\cdot\left[\left(\mu + \frac{\mu_{t_\phi}}{\sigma_\varepsilon}\right)\nabla(\phi\langle\varepsilon\rangle^i)\right] + c_1\left(-\rho\langle\overline{\mathbf{u}'\mathbf{u}'}\rangle^i\nabla\bar{\mathbf{u}}_D\right)\frac{\langle\varepsilon\rangle^i}{\langle k\rangle^i} + c_2c_k\rho\frac{\phi\langle\varepsilon\rangle^i|\bar{\mathbf{u}}_D|}{\sqrt{K}} - c_2\,\rho\phi\frac{\langle\varepsilon\rangle^{i^2}}{\langle k\rangle^i} \tag{17}$$

where $\sigma_k = 1$, $\sigma_\varepsilon = 1.3$, $c_1 = 1.44$, $c_2 = 1.92$, $c_\mu = 0.09$ and $c_k = 0.28$ are non-dimensional constants [24,25].

2.4. Macroscopic energy equations

Similarly, macroscopic energy equations are obtained for both fluid and solid phases by applying time and volume average operators to Eqs. (3) and (4). As in the flow case, volume integration is performed over a REV, resulting in,

$$(\rho c_p)_f\left[\frac{\partial\phi\langle\overline{T_f}\rangle^i}{\partial t} + \nabla\cdot\left\{\phi\left(\langle\bar{\mathbf{u}}\rangle^i\langle\overline{T_f}\rangle^i + \underbrace{\langle{}^i\bar{\mathbf{u}}\,{}^i\overline{T_f}\rangle^i}_{\text{thermal disperson}} + \underbrace{\overline{\langle\mathbf{u}'\rangle^i\langle T_f'\rangle^i}}_{\text{turbulent heat flux}} + \underbrace{\langle\overline{{}^i\mathbf{u}'\,{}^iT_f'}\rangle^i}_{\text{turbulent thermal disperson}}\right)\right\}\right] = \underbrace{\nabla\cdot\left[k_f\nabla\left(\phi\langle\overline{T_f}\rangle^i\right) + \frac{1}{\Delta V}\int_{A_i}\mathbf{n}_ik_f\overline{T_f}\,dA\right]}_{\text{conduction}} + \underbrace{\frac{1}{\Delta V}\int_{A_i}\mathbf{n}_i\cdot k_f\nabla\overline{T_f}\,dA}_{\text{interfacial heat transfer}} \tag{18}$$

where the expansion,

$$\left\langle\overline{\mathbf{u}'T_f'}\right\rangle^i = \left\langle\overline{(\langle\mathbf{u}'\rangle^i + {}^i\mathbf{u}')(\langle T_f'\rangle^i + {}^iT')}\right\rangle^i = \overline{\langle\mathbf{u}'\rangle^i\langle T_f'\rangle^i} + \left\langle\overline{{}^i\mathbf{u}'\,{}^iT_f'}\right\rangle^i \tag{19}$$

has been used in light of the double decomposition concept given by Eqs. (7)–(10) [25]. For the solid phase, one has,

$$(\rho c_p)_s\left\{\frac{\partial(1-\phi)\langle\overline{T_s}\rangle^i}{\partial t}\right\} = \underbrace{\nabla\cdot\left\{k_s\nabla\left[(1-\phi)\langle\overline{T_s}\rangle^i\right] - \frac{1}{\Delta V}\int_{A_i}\mathbf{n}_ik_s\overline{T_s}\,dA\right\}}_{\text{conduction}} \underbrace{-\frac{1}{\Delta V}\int_{A_i}\mathbf{n}_i\cdot k_s\nabla\overline{T_s}\,dA}_{\text{interfacial heat transfer}} \tag{20}$$

In (18) and (20), $\langle\overline{T_s}\rangle^i$ and $\langle\overline{T_f}\rangle^i$ denote the intrinsic average temperature of solid and fluid phases, respectively, A_i is the interfacial area within the REV and $\mathbf{n}_i$ is the unit vector normal to the fluid–solid interface, pointing from the fluid towards the solid phase. Eqs. (18) and (20) are the macroscopic energy equations for the fluid and the porous matrix (solid), respectively.

In order to use Eqs. (18) and (20), the underscored terms have to be modeled as a function of the intrinsically averaged temperature of solid phase and fluid, $\langle\overline{T_s}\rangle^i$ and $\langle\overline{T_f}\rangle^i$. To accomplish this, a gradient type diffusion model is used for all the terms, in the form,

Author's personal copy

Table 1
Correlations for heat transfer coefficient and fluid-to-solid specific area a_i.

Reference	Correlation	Equation	a_i	Flow regime
Wakao et al. [13]	$\frac{h_i D}{k_f} = 2 + 1.1 Re_D^{0.6} Pr^{1/3}$	(33)	$\frac{6(1-\phi)}{D}$	Laminar
Kuwahara et al. [14]	$\frac{h_i D}{k_f} = \left(1 + \frac{4(1-\phi)}{\phi}\right) + \frac{1}{2}(1-\phi)^{1/2} Re_D Pr^{1/3}$	(34)	$\frac{4(1-\phi)}{D}$	Laminar
Saito and de Lemos [41]	$\frac{h_i D}{k_f} = 0.08\left(\frac{Re_D}{\phi}\right)^{0.8} Pr^{1/3}$	(35)	$\frac{4(1-\phi)}{D}$	Turbulent

$$\text{Turbulent heat flux}: \quad -(\rho c_p)_f \left(\phi \langle \overline{\mathbf{u}'} \rangle^i \langle \overline{T'_f} \rangle^i\right) = \mathbf{K}_t \cdot \nabla \langle \overline{T}_f \rangle^i \tag{21}$$

$$\text{Thermal dispersion}: \quad -(\rho c_p)_f \left(\phi \langle {}^i\overline{\mathbf{u}}\, {}^i\overline{T}_f \rangle^i\right) = \mathbf{K}_{disp} \cdot \nabla \langle \overline{T}_f \rangle^i \tag{22}$$

$$\text{Turbulent thermal dispersion}: \quad -(\rho c_p)_f \left(\phi \left\langle \overline{{}^i\mathbf{u}'\, {}^i T'_f} \right\rangle^i\right) = \mathbf{K}_{disp,t} \cdot \nabla \langle \overline{T}_f \rangle^i \tag{23}$$

$$\text{Local conduction}: \quad \nabla \cdot \left[\frac{1}{\Delta V} \int_{A_i} \mathbf{n}_i k_f \overline{T}_f \, dA\right] = \mathbf{K}_{f,s} \cdot \nabla \langle \overline{T}_s \rangle^i - \nabla \cdot \left[\frac{1}{\Delta V} \int_{A_i} \mathbf{n}_i k_s \overline{T}_s \, dA\right] = \mathbf{K}_{s,f} \cdot \nabla \langle \overline{T}_f \rangle^i \tag{24}$$

where $\mathbf{n}_i$ in (24) as already noted, is the unit vector pointing outwards of the fluid phase. In this work, for simplicity, one assumed that for turbulent flow the overall thermal resistance between the two phases is controlled by the interfacial film coefficient, rather than by the thermal resistance within each phase. As such, the tortuosity coefficients $\mathbf{K}_{f,s}$, $\mathbf{K}_{s,f}$ are here neglected for the sake of simplicity.

The heat transferred between the two phases can be modeled by means of a film coefficient h_i such that,

$$h_i a_i \left(\langle \overline{T}_s \rangle^i - \langle \overline{T}_f \rangle^i\right) = \frac{1}{\Delta V} \int_{A_i} \mathbf{n}_i \cdot k_f \nabla \overline{T}_f \, dA = \frac{1}{\Delta V} \int_{A_i} \mathbf{n}_i \cdot k_s \nabla \overline{T}_s \, dA \tag{25}$$

where $a_i = A_i/\Delta V$ is the surface area per unit volume.

For the above shown expressions, Eqs. (18) and (20) can be written as:

$$\{(\rho c_p)_f \phi\} \frac{\partial \langle \overline{T}_f \rangle^i}{\partial t} + (\rho c_p)_f \nabla \cdot \left(\mathbf{u}_D \langle \overline{T}_f \rangle^i\right) = \nabla \cdot \left\{\mathbf{K}_{eff,f} \cdot \nabla \langle \overline{T}_f \rangle^i\right\} + h_i a_i \left(\langle \overline{T}_s \rangle^i - \langle \overline{T}_f \rangle^i\right) \tag{26}$$

$$\{(1-\phi)(\rho c_p)_s\} \frac{\partial \langle \overline{T}_s \rangle^i}{\partial t} = \nabla \cdot \left\{\mathbf{K}_{eff,s} \cdot \nabla \langle \overline{T}_s \rangle^i\right\} - h_i a_i \left(\langle \overline{T}_s \rangle^i - \langle \overline{T}_f \rangle^i\right) \tag{27}$$

where $\mathbf{K}_{eff,f}$ and $\mathbf{K}_{eff,s}$ are the effective conductivity tensor for fluid and solid, respectively, given by:

$$\mathbf{K}_{eff,f} = [\phi k_f]\mathbf{I} + \mathbf{K}_{f,s} + \mathbf{K}_t + \mathbf{K}_{disp} + \mathbf{K}_{disp,t} \tag{28}$$

$$\mathbf{K}_{eff,s} = [(1-\phi) k_s]\mathbf{I} + \mathbf{K}_{s,f} \tag{29}$$

and $\mathbf{I}$ is the unit tensor.

In order to be able to apply Eq. (26), it is necessary to determine the dispersion and conductivity tensors in Eq. (28), i.e., $\mathbf{K}_{f,s}$, $\mathbf{K}_t$, $\mathbf{K}_{disp}$ and $\mathbf{K}_{disp,t}$. Following Kuwahara and Nakayama [43] and Quintard et al. [12], $\mathbf{K}_{f,s}$ and $\mathbf{K}_{disp}$, are obtained by making use of a unit cell subjected to periodic boundary conditions, where (22) are (24) are numerically resolved. Further, dispersion tensor components are then obtained directly from the microscopic results, for a unit cell, and reads for $Pe_D \geqslant 10$ [43]:

$$\frac{(K_{disp})_{yy}}{k_f} = 0.052(1-\phi)^{0.5} Pe_D, \qquad \text{for transverse dispersion} \tag{30}$$

$$\frac{(K_{disp})_{xx}}{k_f} = 2.1 \frac{Pe_D}{(1-\phi)^{0.1}}, \qquad \text{for longitudinal dispersion} \tag{31}$$

The turbulent heat flux and turbulent thermal dispersion terms, $\mathbf{K}_t$ and $\mathbf{K}_{disp,t}$, which cannot be determined from such a microscopic calculation, are here modeled through the Eddy diffusivity concept, as:

$$\mathbf{K}_t + \mathbf{K}_{disp,t} = \phi (\rho c_p)_f \frac{\nu_{t_\phi}}{\sigma_T} \mathbf{I} \tag{32}$$

where $\sigma_T = 0.9$ is the macroscopic turbulent Prandtl number for the fluid energy equation.

2.5. Interfacial heat transfer, h_i

Wakao et al. [13] proposed a correlation for h_i for closely packed bed and compared results with their experimental data. This correlation reads,

$$\frac{h_i D}{k_f} = 2 + 1.1 Re_D^{0.6} Pr^{1/3} \tag{33}$$

Kuwahara et al. [14] also obtained the interfacial convective heat transfer coefficient for laminar flow, as follows:

$$\frac{h_i D}{k_f} = \left(1 + \frac{4(1-\phi)}{\phi}\right) + \frac{1}{2}(1-\phi)^{1/2} Re_D Pr^{1/3}, \quad \text{valid for } 0.2 < \phi < 0.9 \tag{34}$$

Eq. (34) is based on porosity dependency and is valid for packed beds of particle diameter D.

Following this same methodology, in which the porous medium is considered an infinite number of solid square rods, Saito and de Lemos [41] proposed a correlation for obtaining the interfacial heat transfer coefficient for turbulent flow as,

$$\frac{h_i D}{k_f} = 0.08\left(\frac{Re_D}{\phi}\right)^{0.8} Pr^{1/3}; \quad \text{for } 1.0 \times 10^4 < \frac{Re_D}{\phi} < 2.0 \times 10^7, \quad \text{valid for } 0.2 < \phi < 0.9 \tag{35}$$

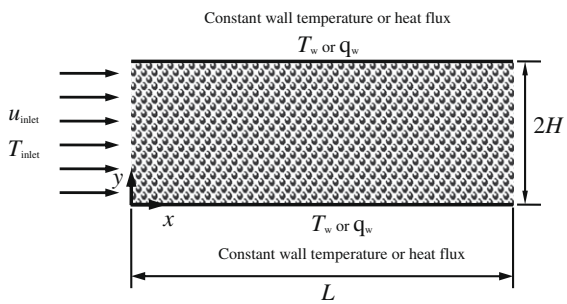

Fig. 1. Geometry under investigation and coordinate system.

Author's personal copy

Table 1 shows three variant correlations for the fluid to solid heat transfer coefficient h_i and the specific surface area of the porous medium a_i, which appears in both energy equations.

The Nusselt number for a porous medium is calculated for both the fluid and solid phases and is defined as,

Fluid phase Nusselt number,

$$Nu_f = -\frac{2H}{T_w - T_{mf}}\left(\frac{\partial\langle T_f\rangle^i}{\partial y}\right) \tag{36}$$

Solid phase Nusselt number,

$$Nu_s = -\frac{2H}{T_w - T_{ms}}\left(\frac{\partial\langle T_s\rangle^i}{\partial y}\right) \tag{37}$$

where T_{mf} and T_{ms} are the average temperature of the fluid and the solid phase, respectively, and are defined as follows:

$$T_{mf} = \frac{\int uT_f\,dy}{u_B H} \tag{38}$$

$$T_{ms} = \frac{\int T_s\,dy}{H} \tag{39}$$

The solid-phase Nusselt number, Nu_s, was proposed by Alazmi and Vafai [45] and refers to a non-dimensional temperature gradient for the solid phase at the wall. This concept has also been applied in reference [42] for laminar flows.

Non-dimensional local and cross-section averaged temperatures, for both phases, are defined as,

$$\theta_{(s,f)} = \frac{T_w - T_{(s,f)}}{T_w - T_{inlet_{(s,f)}}} \tag{40}$$

$$\Theta_{(s,f)} = \frac{T_{m_{(s,f)}} - T_{inlet_f}}{T_{inlet_s} - T_{inlet_f}} \tag{41}$$

Temperature gradients at wall, necessary to calculate the fluid Nusselt number in Eq. (36), are evaluated via the High *Re* Turbulence Model, which makes use of wall functions as follows:

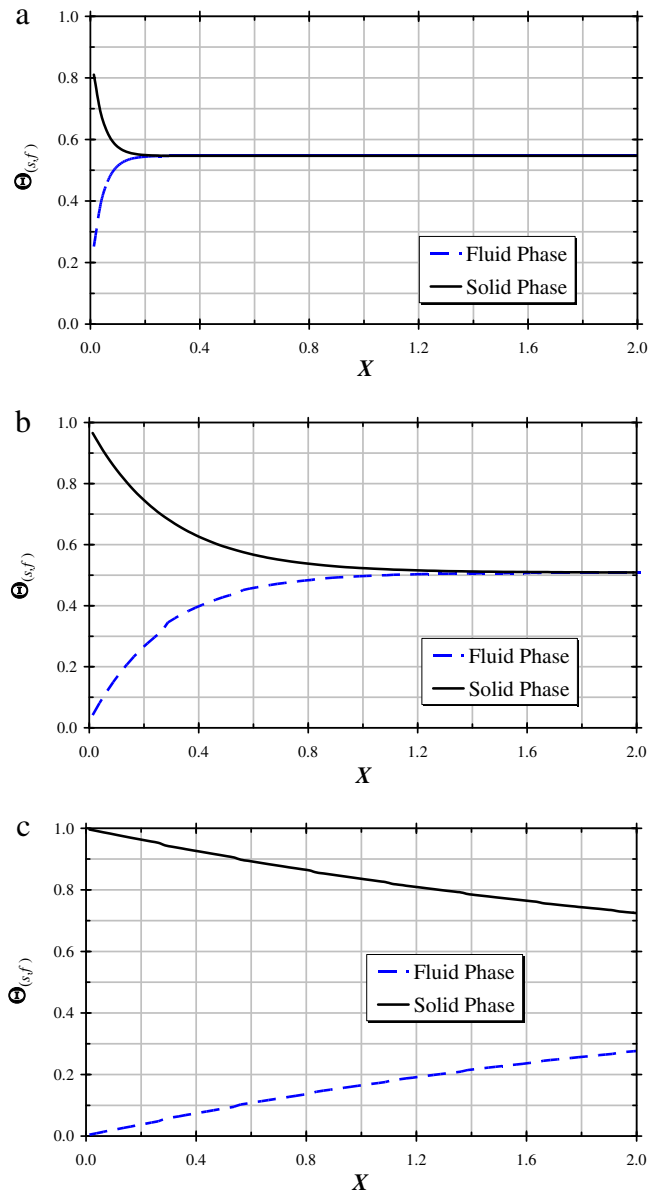

Fig. 2. Fluid and solid cross-sectional averaged temperatures along the flow, $Da = 10^{-4}$, $Re_D = 100$, $\phi = 0.6$, $D/H = 1.03 \times 10^{-1}$, $k_s/k_f = 25$: (a) $h_{eff} = 10h_i$; (b) $h_{eff} = h_i$; and (c) $h_{eff} = 0.1h_i$.

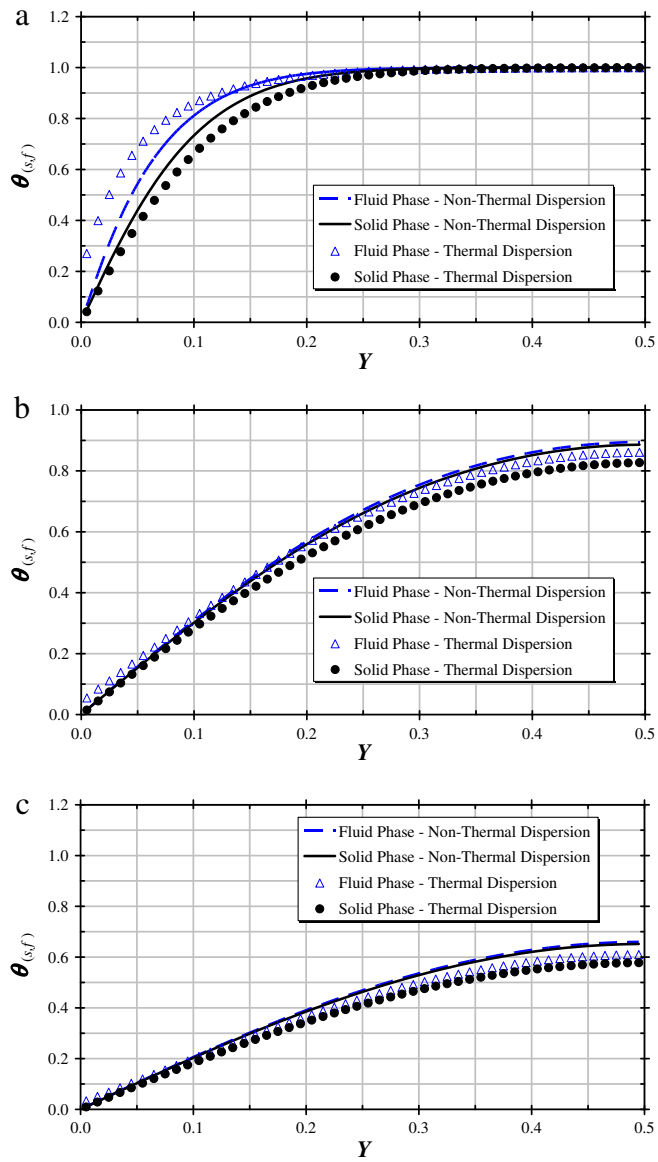

Fig. 3. Effect of thermal dispersion on local non-dimensional temperatures, $Da = 10^{-4}$, $Re_D = 100$, $\phi = 0.6$, $D/H = 1.03 \times 10^{-1}$, $k_s/k_f = 25$: (a) $X = 0.1$, (b) $X = 0.5$, and (c) $X = 1$.

Author's personal copy

$$\frac{\bar{u}}{u_\tau} = \frac{1}{\kappa}\ln(y^+\mathrm{E}), \quad k = \frac{u_\tau^2}{c_\mu^{1/2}}, \quad \varepsilon = \frac{c_\mu^{3/4}k_\mathrm{w}^{3/2}}{\kappa y_\mathrm{w}},$$

$$q_\mathrm{w} = \frac{(\rho c_p)_\mathrm{f} c_\mu^{1/4} k_\mathrm{w}^{1/2}(\overline{T} - T_\mathrm{w})}{\left(\frac{\sigma_t}{\kappa}\ln(y_\mathrm{w}^+) + c_\mathrm{Q}(Pr)\right)} \tag{42}$$

where $u_\tau = \left(\frac{\tau_\mathrm{w}}{\rho}\right)^{1/2}$, $y_\mathrm{w}^+ = \frac{y_\mathrm{w} u_\tau}{\nu}$, $c_\mathrm{Q} = 12.5Pr^{2/3} + 2.12\ln(Pr) - 5.3$ for $Pr > 0.5$.

In Eq. (42), q_w is wall heat flux, u_τ is wall-friction velocity, y_w is the coordinate normal to wall and κ is the von Kármán constant. Further, in Eq. (42) E is equal to 9.0 for smooth walls.

3. Numerical method

The problem under investigation is a flow through a channel completely filled with a porous medium, as shown in Fig. 1. Boundary conditions and periodic constraints for turbulent flows in porous media are similar to the clear channel flow.

The numerical method utilized to discretize the flow and energy equations in the unit cell is the Finite Control Volume approach. The SIMPLE method of Patankar [46] was used for handling the velocity–pressure coupling. Convergence was monitored in terms of the normalized residue for each variable. The maximum residue allowed for convergence check was set to 10^{-9}, being the variables normalized by appropriate reference values.

4. Results and discussion

Results below were obtained after extensive testing on grid size independence and search for optimal relaxation parameters. Due to lack of space here, the interest reader is referred to previous work where such studies are presented in detail [26–39].

4.1. Laminar flow

Exact solutions for thermal non-equilibrium of laminar flow in porous media are presented in [44] and comparisons with the

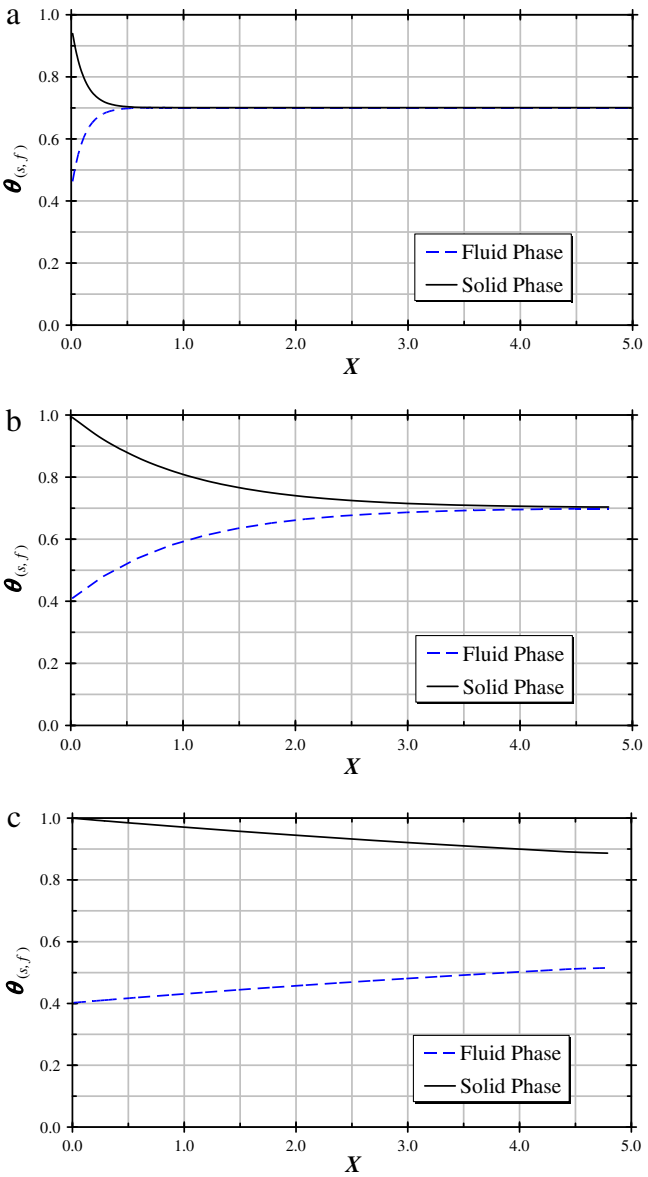

Fig. 4. Fluid and solid cross-sectional averaged temperatures along the flow, $Da = 10^{-4}$; $Re_\mathrm{D} = 5 \times 10^4$, $\phi = 0.6$; $D/H = 1.03 \times 10^{-1}$; $k_s/k_f = 25$: (a) $h_\mathrm{eff} = 10h_i$, (b) $h_\mathrm{eff} = h_i$, and (c) $h_\mathrm{eff} = 0.1h_i$.

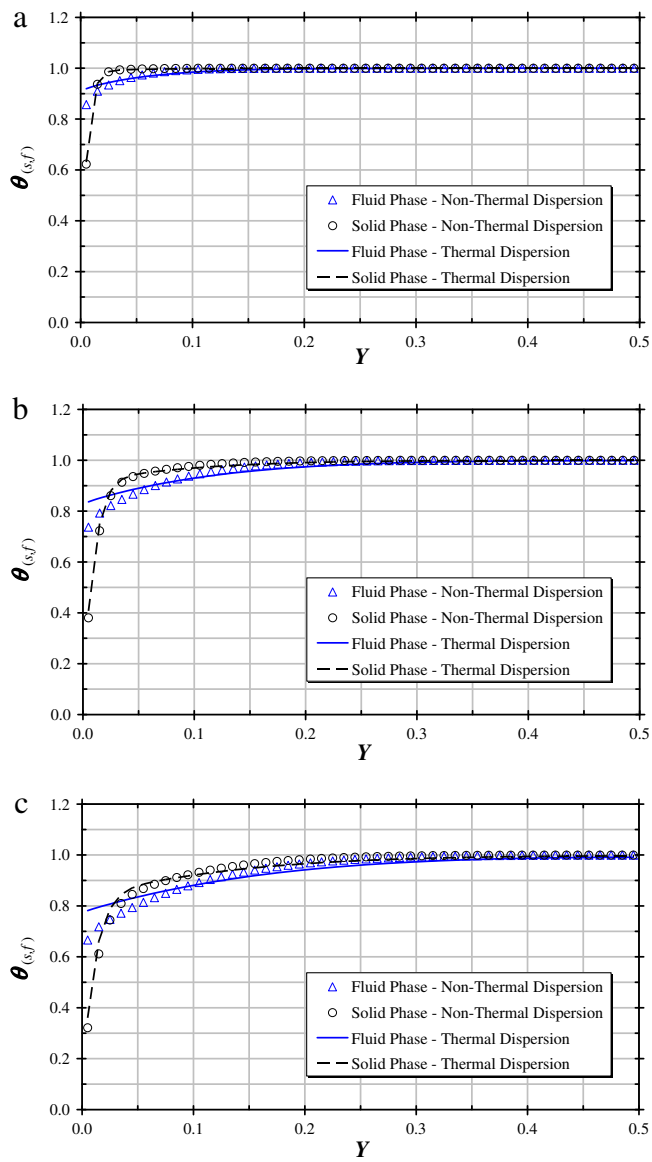

Fig. 5. Effect of thermal dispersion on local non-dimensional temperatures, $Da = 10^{-4}$, $Re_\mathrm{D} = 5 \times 10^4$, $\phi = 0.6$; $D/H = 1.03 \times 10^{-1}$, $k_s/k_f = 25$: (a) $X = 0.1$, (b) $X = 0.5$, and (c) $X = 1$.

Author's personal copy

present simulations were carried out in order to assess the correctness of the code here employed. Due to lack of space, and due to the fact that turbulent flow is the primary subject of this work, such results are here not presented and shall be the subject of a forthcoming paper.

First, in order to verify the correctness of the solutions, a sensitivity study on the value of h_i for laminar flow is presented. It is expected that the higher the interfacial heat transfer coefficient, the smaller the differences between the fluid and the solid temperatures and the faster the fully developed equilibrium temperature is achieved. Temperature distributions for both phases and for the conditions $Da = 10^{-4}$, $Re_D = 100$, $\phi = 0.6$, $D/H = 1.03 \times 10^{-1}$, $k_s/k_f = 25$ and $\theta_f|_{inlet} \neq \theta_s|_{inlet}$ are plotted in Fig. 2 along the non-dimensional coordinate $X = x/H$. The value for Da is calculated as $Da = K/H^2$ where K is the permeability given by [47]

$$K = \frac{D^2\phi^3}{144(1-\phi)^2} \tag{43}$$

or

$$Da = \frac{K}{H^2} = \frac{(D/H)^2\phi^3}{144(1-\phi)^2} \tag{44}$$

Values for D and ϕ are chosen such that a certain Da is obtained, without reflecting necessarily real values of a specific medium.

In Fig. 2 a nominal value for h_i is calculated with correlation (34). An effective value h_{eff} is artificially introduced by modifying this nominal value. The figure indicates that the solid phase is cooled down to the thermal equilibrium temperature as the fluid flows downstream the channel. In Fig. 2, the nominal value for h_i in employed (Fig. 2b) and compared with effective higher (Fig. 2a) and lower (Fig. 2c) h_i values. Corresponding shortening (Fig. 2a) and extension (Fig. 2c) of developing length are correctly calculated.

The effect of thermal dispersion on the temperature profiles, also for the conditions $Da = 10^{-4}$, $Re_D = 100$, $\phi = 0.6$, $D/H = 1.03 \times 10^{-1}$ and $k_s/k_f = 25$, is shown in Fig. 3 at three distinct axial positions X. The thermal dispersion tensor components are given by expressions (31) and (30). It is clearly seen from the figure that

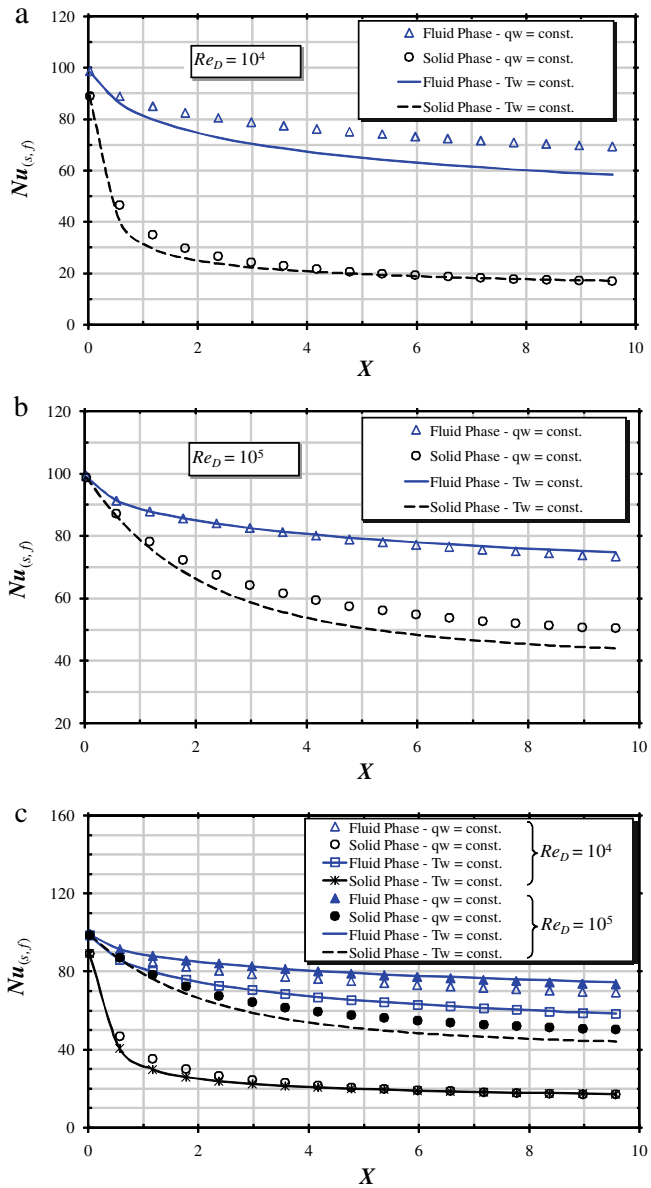

Fig. 6. Effect of Re_D on Nu for turbulent flow, $Da = 10^{-4}$, $\phi = 0.6$, $D/H = 1.03 \times 10^{-1}$, $k_s/k_f = 25$: (a) $Re_D = 10^4$, (b) $Re_D = 10^5$, and (c) Both Re_D.

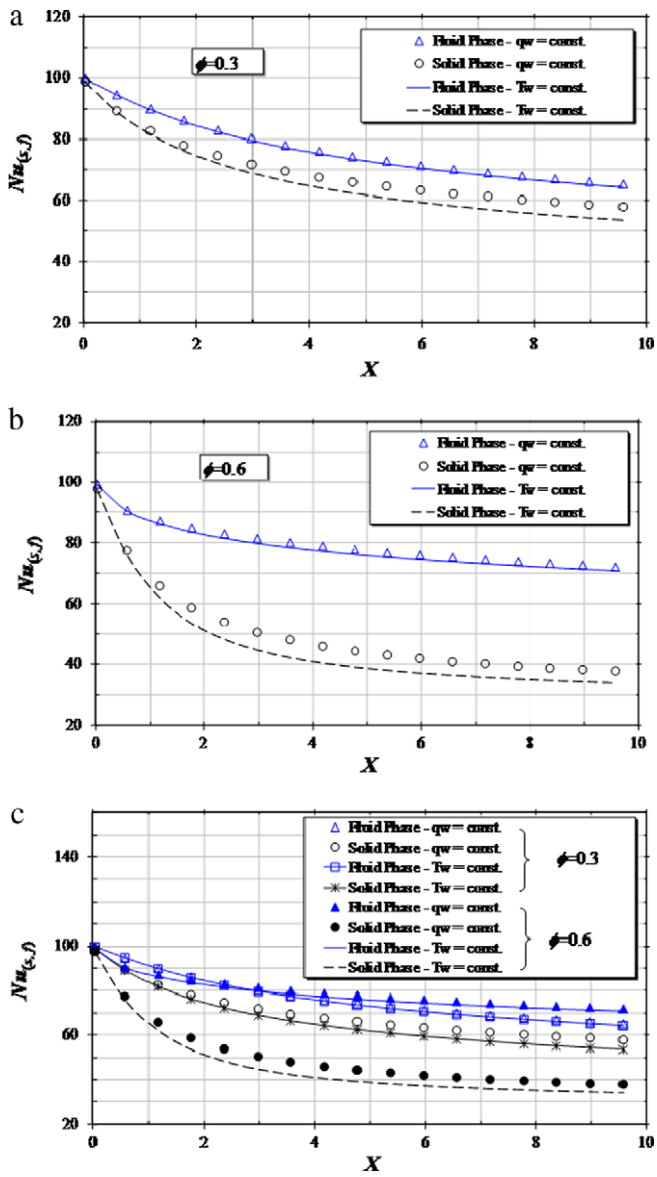

Fig. 7. Effect of ϕ on Nu for turbulent flow, $Da = 10^{-4}$; $Re_D = 5 \times 10^4$; $D/L = 1.03 \times 10^{-2}$; $k_s/k_f = 25$: (a)$\phi = 0.3$, (b) $\phi = 0.6$, and (c) Both φ

Author's personal copy

the differences in temperature between the solid and fluid phases temperatures at transverse positions are larger when $\mathbf{K}_{disp}$ is considered, particularly at the channel entrance region, $X = 0.1$ (Fig. 3a). An explanation for such behavior is that the thermal dispersion is an additional transport mechanism acting on the fluid phase, yielding flatter cross-sectional profiles for $\langle \overline{T}_f \rangle^i$, resulting in larger differences from corresponding local values of $\langle \overline{T}_s \rangle^i$. The figure also indicates that such differences are reduced along the flow (Fig. 3b and c) as the two phases exchange heat through their interstitial area.

4.2. Turbulent flow

Also for turbulent flow ($Re_D = 5 \times 10^4$), a sensitive analysis on the value of h_i is performed in order to evaluate the correctness of code programming. Fig. 4 shows results for the cross-section averaged temperatures for both the solid and fluid phases. As in the case of laminar flow (Fig. 2), a nominal value for h_i in employed in Fig. 4b and compared with artificially increased (Fig. 4a) and reduced (Fig. 4c) values of the interfacial film coefficient. Also for turbulent flow, shorter (Fig. 4a) and larger (Fig. 4c) developing lengths correspond to higher and lower values for h_i, respectively, indicating that physically realistic results for temperatures are obtained.

Next, the effect of introducing $\mathbf{K}_{disp}$ in the calculations for turbulent flow is presented is Fig. 5, for the conditions $Da = 10^{-4}$, $Re_D = 5 \times 10^4$, $D/H = 1.03 \times 10^{-1}$, $k_s/k_f = 25$ and $\phi = 0.6$. The differences between the solid and fluid phase temperature profiles are greater when thermal dispersion is incorporated in the macroscopic model, particularly in the near wall region ($Y < 0.1$), which embraces the boundary layer that is much thinner than for laminar flows cases, see Fig. 3 for comparison. Therefore, here also the role of the additional mechanism of dispersion is to promote diffusion across the cross-section of the channel, leading to flatter $\langle \overline{T}_f \rangle^i$ profiles and larger temperature differences from corresponding local values of $\langle \overline{T}_s \rangle^i$. Effects of Reynolds number, Re_D, porosity, ϕ, non-dimensional particle diameter, D/L, and solid-to-fluid thermal conductivity, k_s/k_f, on temperature behavior are shown next.

Fig. 6 shows the effect of the Reynolds number and boundary condition on Nu. One can note in the figure that an increase in Re_D results in an increase in Nusselt, for all cases, as expected. For high values of Re_D, Nu_f and Nu_s are closer to each other when compared with similar computations for $Re_D = 10^5$ (Fig. 6b). Fig. 6c shows a comparison of all cases and indicates that Nu_f attains higher values than Nu_s, along the flow direction.

In Fig. 7a and b, the effect of porosity ϕ on Nu is presented. An increase in porosity causes the solid phase Nusselt number to decrease whereas Nu_f in augmented, for both boundary condition types. Increase in this difference for low porosity medium could be explained by noting that a higher ϕ gives a lower h_i, according to Eq. (35), as well as a lower a_i, as seen in Table 1. Their product, $h_i a_i$, is proportional to the heat transfer between phases, as shown by the two energy equations (26) and (27). Consequently, a high porosity medium will have the intensity of energy transfer between phases reduced, reflecting in the temperature fields and, ultimately, on the calculated Nu values.

Fig. 8 shows the effect of the non-dimensional particle diameter D/L on Nusselt, for a fixed porosity. In general, an increase in the particle diameter D/L results in an increase in Nusselt, for both phases and both boundary condition types (Fig. 8a and b). When porosity is constant and the thermal dispersion effects are omitted, the particle diameter only affects h_i and a_i (see Eq. (35) and Table 1). A reduced value for D/L with a constant ϕ increases the interstitial area, promoting the exchange of energy between phases, leading to a reduction of the temperature gradients in the wall region, which ultimately reflects on the Nu values. Fig. 8c compiles such findings and shows for turbulent flow, small differences on Nu prevail in spite of the boundary condition type used.

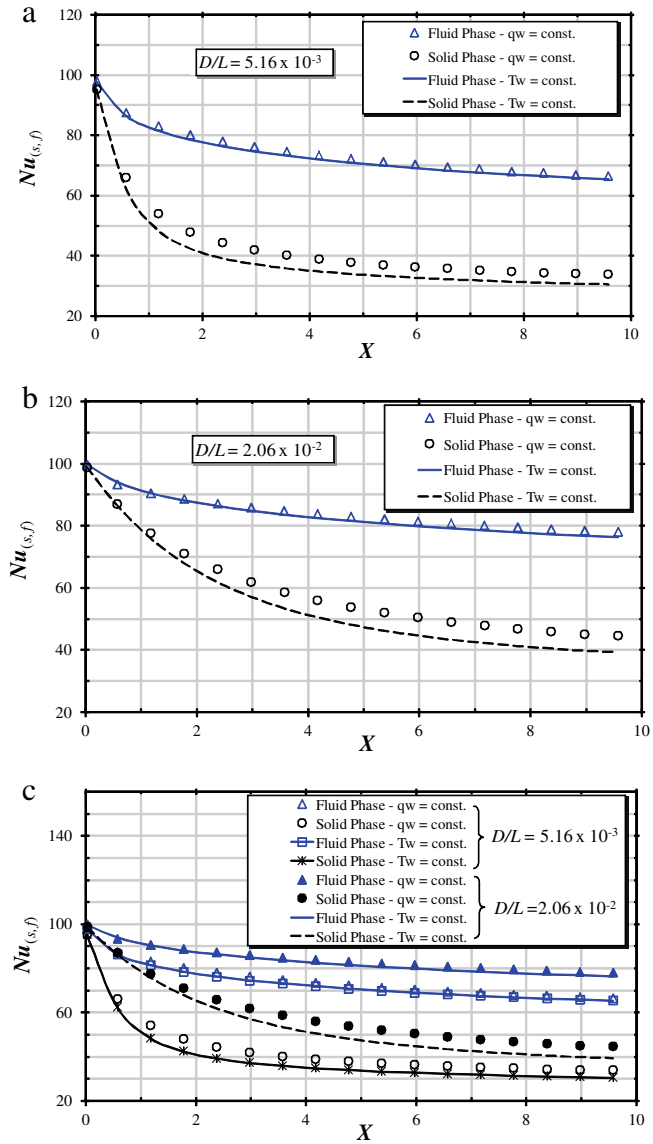

Fig. 8. Effect of D/L on Nu for turbulent flow, $Re_D = 5 \times 10^4$; $\phi = 0.6$; $k_s/k_f = 25$: (a) $D/L = 5.16 \times 10^{-3}$, (b) $D/L = 2.06 \times 10^{-2}$, and (c) Both D/L.

Effects of the ratio k_s/k_f is presented in Fig. 9. All computations made so far were obtained with $k_s/k_f = 25$ and when one compares Fig. 9a and 9b, one can note that the lower such ratio, the closer are the values for the Nusselt numbers, regardless of the boundary condition used. When the fluid and the solid conduct heat at rates of the same order, their temperatures levels do not differ much, with reflection on the proximity of corresponding Nusselt numbers. Further, differences between the Nusselt numbers for q_w = const. and T_w = const. are reduced for the solid, when k_s/k_f is large, and increased for the fluid, for small values of k_s/k_f (Fig. 9c).

5. Conclusions

This paper investigated the behavior of a two-energy equation model to simulate flow and heat transfer in a porous bed. Effects of thermal dispersion, Reynolds number, particle diameter, poros-

Author's personal copy

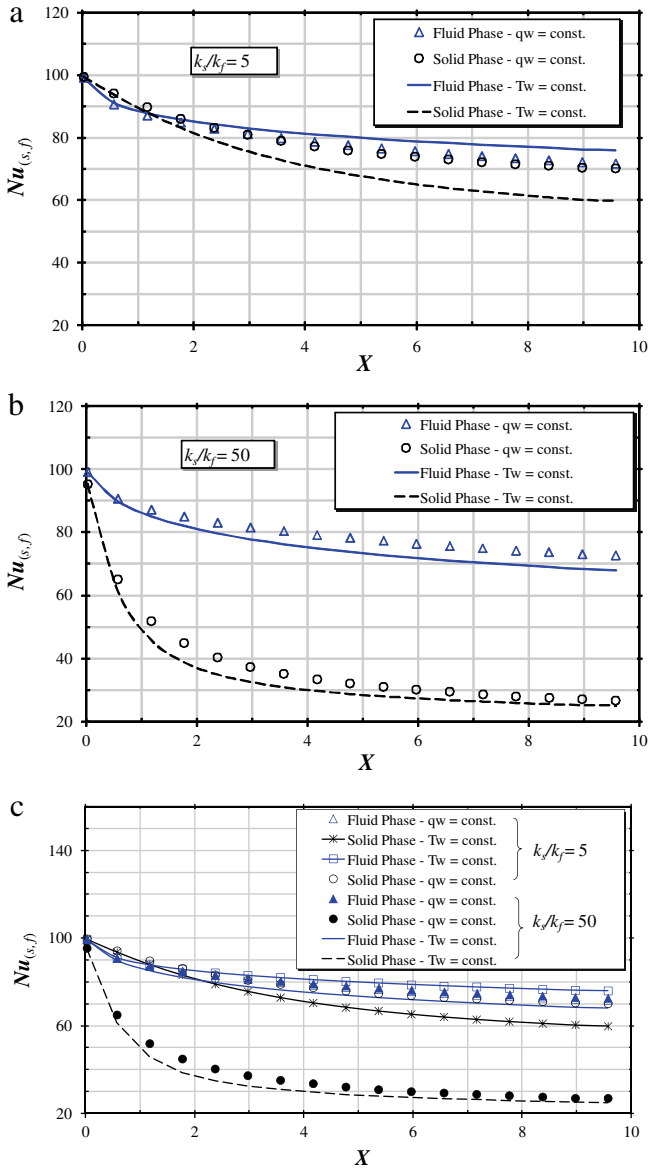

Fig. 9. Effect of k_s/k_f on Nu for turbulent flow, $Da = 10^{-4}$, $Re_D = 5 \times 10^4$, $\varphi = 0.6$, $D/H = 1.03 \times 10^{-1}$: (a) $k_s/k_f = 5$, (b) $k_s/k_f = 50$.

ity and solid-to-fluid thermal conductivity ratio were investigated. The following conclusions can be drawn:

(1) For laminar flow, the thermal dispersion mechanism promotes energy exchange in the fluid phase, leading to larger local temperature differences when the solid and the fluid temperature are compared along the channel cross-section, particularly at the entry region.
(2) For turbulent flow, the effect of including the thermal dispersion mechanism is concentrated in the region close to the wall, within the boundary layer, where such temperature differences are pronounced.
(3) Increase in Re number causes values for Nu of both phases to increase and to approach each other.
(4) An increase in porosity causes the solid phase Nusselt number to decrease whereas Nu_f in augmented, for both boundary condition types. A high porosity medium will have the intensity of energy transfer between phases reduced, reflecting in the temperature fields and, ultimately, on the calculated Nu values.
(5) A reduced value for D/L with a constant porosity increases the interstitial area, promoting the exchange of energy between phases, leading to a reduction of the temperature gradients in the wall region. In general, an increase in the particle diameter results in an increase in Nusselt, for both phases and both boundary conditions.
(6) The thermal conductivity ratio k_s/k_f causes the most effect on Nusselt numbers, and the grater the ratio, the most wider apart are Nu_s and Nu_f, with a reduction of Nusselt for the solid phase.

Acknowledgments

The authors express their gratitude to CNPq and FAPESP, Brazil, for their invaluable financial support during the course of this research.

References

[1] T.E.W. Schumann, Heat transfer: liquid flowing through a porous prism, J. Franklin Inst. 208 (1929) 405–416.
[2] K. Vafai, M. Sozen, Analysis of energy and momentum transport for fluid flow through a porous bed, J. Heat Transfer 112 (1990) 690–699.
[3] A. Amiri, K. Vafai, Analysis of dispersion effects and non-thermal equilibrium, non-Darcian, variable porosity incompressible flow through porous media, Int. J. Heat Mass Transfer 30 (1994) 939–954.
[4] S. Whitaker, Improved constraints for the principle of local thermal equilibrium, Ind. Eng. Chem. Res. 30 (1991) 983–997.
[5] M. Quintard, S. Whitaker, One- and two-equation models for transient diffusion processes in two-phase systems, Advances in Heat Transfer, vol. 23, Academic Press, New York, 1993.
[6] M. Quintard, S. Whitaker, Local thermal equilibrium for transient heat conduction: theory and comparison with numerical experiments, Int. J. Heat Mass Transfer 38 (1995) 2779–2796.
[7] C.T. Hsu, A closure model for transient heat conduction in porous media, J. Heat Transfer 121 (1999) 733–739.
[8] M. SÖZEN, K. VAFAI, Analysis of the non-thermal equilibrium condensing flow of a gas through a packed bed, Int. J. Heat Mass Transfer 33 (6) (1990) 1247–1261.
[9] M. Kaviany, Principles of Heat Transfer in Porous Media, second ed., Springer, New York, 1995.
[10] M. Quintard, Modeling local non-equilibrium heat transfer in porous media, in: Proceedings of the 11th International Heat Transfer Conference, Kyongyu, Korea, vol. 1, 1998, pp. 279–285.
[11] D.B. Ingham, I. Pop, Transport Phenomena in Porous Media, Elsevier, Amsterdam, 1998. pp. 103–129.
[12] M. Quintard, M. Kaviany, S. Whitaker, Two-medium treatment of heat transfer in porous media: numerical results for effective properties, Adv. Water Resour. 20 (1997) 77–94.
[13] N. Wakao, S. Kaguei, T. Funazkri, Effect of fluid dispersion coefficients on particle-to-fluid heat transfer coefficients in packed bed, Chem. Eng. Sci. 34 (1979) 325–336.
[14] F. Kuwahara, M. Shirota, A. Nakayama, A numerical study of interfacial convective heat transfer coefficient in two-energy equation model for convection in porous media, Int. J. Heat Mass Transfer 44 (2001) 1153–1159.
[15] M.B. Saito, M.J.S. de Lemos, Interfacial heat transfer coefficient for non-equilibrium convective transport in porous media, Int. Commun. Heat Mass Transfer 32 (5) (2005) 667–677.
[16] W.G. Gray, P.C.Y. Lee, On the theorems for local volume averaging of multiphase system, Int. J. Multiphase Flow 3 (1977) 333–340.
[17] H.C. Chan, W.C. Huang, J.M. Leu, C.J. Lai, Macroscopic modeling of turbulent flow over a porous medium, Int. J. Heat Fluid Flow 28 (5) (2007) 1116–1157.
[18] H.C. Chan, J.M. Leu, C.J. Lai, Velocity and turbulence field around permeable structure: comparisons between laboratory and numerical experiments, J. Hydraul. Res. 45 (2) (2007) 216–226.
[19] M.J.S. de Lemos, M.H.J. Pedras, Recent mathematical models for turbulent flow in saturated rigid porous media, J. Fluids Eng. 123 (2001) 935–940.
[20] A. Nakayama, F. Kuwahara, A macroscopic turbulence model for flow in a porous medium, J. Fluids Eng. 121 (2) (1999) 427–433.
[21] A. Nakayama, F. Kuwahara, A general macroscopic turbulence model for flows in packed beds, channels, pipes, and rod bundles, J. Fluids Eng. 130 (10) (2008) 101–205.
[22] M.H.J. Pedras, M.J.S. de Lemos, On the definition of turbulent kinetic energy for flow in porous media, Int. Commun. Heat Mass Transfer 27 (2) (2000) 211–220.
[23] M.H.J. Pedras, M.J.S. de Lemos, Simulation of turbulent flow in porous media using a spatially periodic array and a low-Re two-equation closure, Numer. Heat Transfer A 39 (1) (2001) 35–59.
[24] M.H.J. Pedras, M.J.S. de Lemos, Computation of turbulent flow in porous media using a low Reynolds k–ε model and an infinite array of transversally-displaced elliptic rods, Numer. Heat Transfer Part A 43 (6) (2003) 585–602.

Author's personal copy

[25] B.E. Launder, D.B. Spalding, The numerical computation of turbulent flows, Comput. Meth. Appl. Mech. Eng. 3 (1974) 269–289.
[26] F.D. Rocamora Jr., M.J.S. de Lemos, Analysis of convective heat transfer of turbulent flow in saturated porous media, Int. Commun. Heat Mass Transfer 27 (6) (2000) 825–834.
[27] M.J.S. de Lemos, E.J. Braga, Modeling of turbulent natural convection in saturated rigid porous media, Int. Commun. Heat Mass Transfer 30 (5) (2003) 615–624.
[28] E.J. Braga, M.J. S de Lemos, Turbulent natural convection in a porous square cavity computed with a macroscopic k–ε model, Int. J. Heat and Mass Transfer 47 (26) (2004) 5639–5650.
[29] E.J. Braga, M.J.S. de Lemos, Heat transfer in enclosures having a fixed amount of solid material simulated with heterogeneous and homogeneous models, Int. J. Heat Mass Transfer 48 (23–24) (2005) 4748–4765.
[30] E.J. Braga, M.J.S. de Lemos, Laminar natural convection in cavities filled with circular and square rods, Int. Commun. Heat Mass Transfer 32 (10) (2005) 1289–1297.
[31] E.J. Braga, M.J.S. de Lemos, Turbulent heat transfer in an enclosure with a horizontal porous plate in the middle, J. Heat Transfer 128 (2006).
[32] M.J.S. de Lemos, M.S. Mesquita, Turbulent mass transport in saturated rigid porous media, Int. Commun. Heat Mass Transfer 30 (1) (2003) 105–113.
[33] M.J.S. de Lemos, L.A. Tofaneli, Modeling of double-diffusive turbulent natural convection in porous media, Int. J. Heat Mass Transfer 47 (19–20) (2004) 4221–4231.
[34] M. Assato, M.J.H. Pedras, M.J.S. de Lemos, Numerical solution of turbulent channel flow past a backward-facing-step with a porous insert using linear and non-linear k–ε models, J. Porous Media 8 (1) (2005) 13–29.
[35] N.B. Santos, M.J.S. de Lemos, Flow and heat transfer in a parallel-plate channel with porous and solid baffles, Numer. Heat Transfer Part A 49 (5) (2006) 471–494.
[36] R.A. Silva, M.J.S. de Lemos, Numerical analysis of the stress jump interface condition for laminar flow over a porous layer, Numer. Heat Transfer Part A 43 (6) (2003) 603–617.
[37] R.A. Silva, M.J.S. de Lemos, Turbulent flow in a channel occupied by a porous layer considering the stress jump at the interface, Int. J. Heat Mass Transfer 46 (26) (2003) 5113–5121.
[38] M.J.S. de Lemos, Turbulent kinetic energy distribution across the interface between a porous medium and a clear region, Int. Commun. Heat Mass Transfer 32 (1–2) (2005) 107–115.
[39] M.J.S. de Lemos, R.A. Silva, Turbulent flow over a layer of a highly permeable medium simulated with a diffusion-jump model for the interface, Int. J. Heat Mass Transfer 49 (3–4) (2006) 546–556.
[40] M.J.S. de Lemos, F.D. Rocamora, Turbulent transport modeling for heated flow in rigid porous media, in: Proceedings of the 12th International Heat Transfer Conference, Grenoble, France, August 18–23, 2002, pp. 791–795.
[41] M.B. Saito, M.J.S. de Lemos, A correlation for interfacial heat transfer coefficient for turbulent flow over an array of square rods, J. Heat Transfer 128 (2006) 444–452.
[42] M.B. Saito, M.J.S. de Lemos, Laminar heat transfer in a porous channel simulated with a two-energy equation model, Int. Commun. Heat Mass Transfer 36 (2009) 1002–1007.
[43] F. Kuwahara, A. Nakayama, H. Koyama, A numerical study of thermal dispersion in porous media, J. Heat Transfer 118 (1996) 756–761.
[44] A. Nakayama, F. Kuwahara, M. Sugiyama, Int. J. Heat Mass Transfer 44 (22) (2001) 4375–4379.
[45] B. Alazmi, K. Vafai, Analysis of variants within the porous media transport models, J. Heat Transfer 122 (2000) 303–326.
[46] S.V. Patankar, Numerical Heat Transfer and Fluid Flow, Hemisphere, Washington, DC, 1980.
[47] S. Ergun, Fluid flow through packed columns, Chem. Eng. Proc. 48 (1952) 89–94.